Anisotropic electron diffusion and weak localization in Cu/Al multilayers

A. N. Fadnis
Department of Physics, Indiana University, Bloomington, Indiana 47405

M. L. Trudeau and A. Joly
Materials Technology, Institut de Recherche d'Hydro Quebec (IREQ), Varennes, Quebec; Canada, J3X 1S1

David V. Baxter
Department of Physics, Indiana University, Bloomington, Indiana 47405
(Received 23 March 1993; revised manuscript received 14 July 1993)

Weak localization (WL) was investigated in a series of sputtered Cu/Al multilayers by measuring their transverse magnetoresistance for temperatures between 2.5 and 20 K in fields up to 8 T. Samples of different resistivities were obtained by varying the individual thicknesses of Al and Cu layers, and some were doped with tungsten in order to enhance the spin-orbit scattering. In each case the magnetoresistance was measured for two orientations of the magnetic field—parallel and perpendicular to the plane of the film. The data were analyzed using Kawabata's theory for the magnetoresistance due to WL, and modified to account for anisotropy following the work of Bhatt, Wolfe, and Ramakrishnan. We also found it necessary to include a conventional $(\omega_c\tau)^2$ contribution in order to account for the data at high fields. Application of this theory to the observed magnetoresistance for the two orientations of the field yielded a measure of the transport anisotropy ratio $\delta = (D_{xy}/D_z)$. For the samples studied, δ ranged from 1 to more than 2, with anisotropy being largest for the highest conductivity sample.

I. INTRODUCTION

Metallic multilayers have attracted a large amount of interest lately due to their unique x-ray scattering properties, and their ability to combine contrasting materials properties on very fine length scales.[1–3] Such materials also provide a powerful tool for the study of metallic interfaces due to the large concentration of interfaces which they contain. The question of how electrons are scattered at interfaces is one of both fundamental and technological interest. A number of authors have discussed how the scattering of electrons at interfaces may be studied indirectly, by measuring the resistivities of a series of multilayers as a function of modulation wavelength (Λ) and temperature.[4,5] Interpretation of such experiments is, however, complicated considerably by possible changes in the material properties of the individual layers as the Λ is changed (i.e., the distribution of disorder within the bilayers is not fixed as Λ changes). The measurement of anisotropy in transport coefficients offers an additional probe which can help distinguish disorder concentrated at the interfaces from disorder distributed more uniformly through the multilayer. For example, Trivedi and Ashcroft[6] have examined the transport anisotropy using a semiclassical model in which disorder is confined to lamellar regions periodically repeated in an otherwise clean host metal. Their results indicate that the out-of-plane component of resistivity in a multilayer can be as much as two times larger than the in-plane component for samples in which scattering is restricted to periodically arranged lamellar regions. Some workers have tried to measure the ratio of the in- and out-of-plane components of the resistivity in metallic multilayers directly by making the current flow parallel and perpendicular to the plane of the film, respectively.[7] However, the very small values of resistance in the direction perpendicular to the film, interference from the resistance of the contact interface, and ill-defined current geometries make these measurements very difficult.

In this paper we report on measurements of the magnetoresistance due to weak localization (WL) in a series of Cu/Al multilayers and we demonstrate that such measurements are sensitive to the anisotropy of the electron diffusivity. Such measurements therefore hold promise as an alternative means through which the anisotropy of transport in multilayered systems may be measured.

WL induces a small change in the resistivity of disordered conductors due to interference between alternative electron diffusion paths (in particular, paths which self-intersect) through the material.[8,9] Applying a magnetic field changes the sample's resistance by introducing to this interference additional phase shifts proportional to the flux enclosed by the interfering paths. Thus, the measured magnetoresistance depends on the area over which electrons can diffuse in directions perpendicular to the applied field, during times over which they maintain phase coherence. The WL correction to the resistivity depends on two length scales; $L_\phi = \sqrt{D\tau_\phi}$ and $L_{so} = \sqrt{D\tau_{so}}$. Roughly speaking, these are the distances an electron diffuses between inelastic and spin-orbit scat-

tering events, respectively. When a magnetic field is applied, the magnetoresistance is determined by the flux passing through closed loop electron paths, and thus these length scales appear as characteristic field scales ($B_\phi = \frac{\hbar}{4eD\tau_\phi}$ and $B_{so} = \frac{\hbar}{4eD\tau_{so}}$) in the measurement. Viewed another way, the resistance of the sample depends on the relative size of three lengths, L_ϕ, L_{so}, and $l_B = \sqrt{\hbar/4eB}$. Of these three lengths, L_ϕ depends primarily on temperature, L_{so} depends primarily on the average atomic number of the constituents in the sample, and l_B, of course, depends on the applied magnetic field. Over the last several years this result has been used to measure a variety of solid state phenomena, ranging from spin-spin scattering rates in Kondo systems[10] to interfacial uniformity in semiconductor inversion layers,[11] and the resistivity of quasicrystals.[12]

We exploit the phenomenon to determine the anisotropy of the electron diffusivity in a multilayer by measuring the magnetoresistance for two different orientations of the magnetic field, namely, parallel and perpendicular to the plane of the film. Anisotropy in the diffusivity appears as different values for the characteristic field scales, B_ϕ and B_{so}, for the two field orientations. The essential physics behind the experiment is represented in schematic form in Fig. 1. A number of groups have considered the WL phenomenon in multilayers and other anisotropic media recently;[13–15] however, for the most part these studies have considered only the relative size of the WL correction for different orientations of the current, and a fixed orientation for the magnetic field. Szott, Jedrezejek, and Kirk[16] were the first to use WL to investigate anisotropy in such systems, through careful consideration of the size of the magnetoresistance measured in a $GaAs/Al_xGa_{1-x}As$ superlattice in a perpendicular field. We go beyond this earlier work by using two different orientations of the magnetic field, thereby increasing our sensitivity to the point where

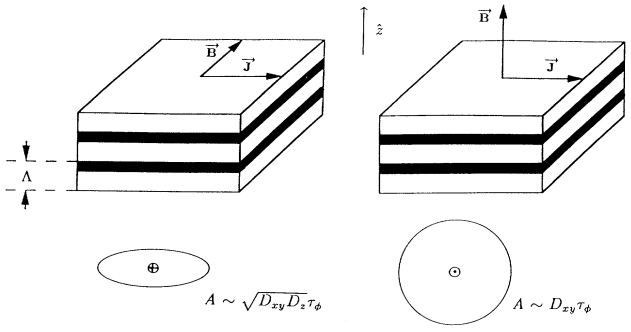

FIG. 1. Schematic representation showing the relative orientation of the magnetic field with the sample and the current direction. Here **B** and **J** denote the magnetic field and the current density, respectively. Note that **J** is always in the plane of the film, and perpendicular to **B**. For a given value of the applied field, the anisotropy of the electron diffusivity causes the average flux enclosed by the diffusion paths contributing to WL to be different for different field orientations. This results in an orientation dependence of the field scales B_{so} and B_ϕ.

the anisotropy in a metallic multilayer may be measured. Cherradi *et al.*[14] have studied the 2D-3D (where 2D denotes two dimensional) crossover in Au/Si multilayers with diminishing Si layer thicknesses, by measuring their magnetoresistance for two different orientations of magnetic field. Their results, as expected, indicate that in cases where the Au layers are strongly coupled by tunneling through thin Si layers (the 3D case), the anisotropy is much smaller than it is when the Au layers are isolated by thick Si layers (the 2D case). Using these experiments, therefore, it was possible to obtain a qualitative picture of the crossover from 2D to 3D. However, these authors did not obtain any quantitative measure of anisotropy in 3D systems.

Details of the WL theory used to analyze our data are presented in the Appendix. We use a theory which is appropriate to anisotropic systems, but which takes no explicit account of the layered nature of our samples. A theory of WL suitable for superlattices has been developed;[13] however, in limits which apply to our samples this theory essentially reduces to the more straightforward anisotropic theory presented in the Appendix. In our experiment the overall current flow is always along the film, which simplifies the experiment compared to a more direct measurement of anisotropy. For both field orientations we keep the current direction transverse to the field in order to avoid interference from possible differences between the longitudinal and transverse magnetoresistance.[17]

The Cu/Al interface is one that has been studied quite extensively due to its potential importance for device applications.[18,19] For our purposes the Cu/Al system has the added advantage that both constituents are readily available in sufficiently pure form for our measurements. A concentration of magnetic impurities as low as 20 parts per million is sufficient to alter significantly the magnetoresistance, so this is a prime consideration.[20] It is our hope that the technique will be found applicable to other systems as well, thereby providing a probe for studying the scattering of electrons at interfaces.

II. EXPERIMENT

The samples were made by planar magnetron sputtering onto kapton or sapphire substrates in a deposition chamber with a base pressure (with the high vacuum pump throttled, and a liquid nitrogen trap filled) of 5×10^{-8} Torr. The substrates were held on a carousel which could sequentially position the substrates over the Cu and Al sputtering guns. Using a third source, mounted between the Cu and Al sources, some samples were doped with very small amounts of W (less than a monolayer) at the Al-Cu interfaces in order to enhance spin-orbit scattering. When doping, the deposition sequence was such that only one of the two pairs of samples made in the run was exposed to the W gun, and therefore had W at the interfaces. The samples in the other pair received the same Cu and Al exposures but no W, and therefore served as low spin-orbit controls. The targets were purchased commercially and had a specified purity of Cu 99.999%, Al 99.999%, and W 99.95%. The target

to substrate distance was roughly 15 cm and the sputtering pressure was 6.4 mTorr of Ar (5N5 purity). The Cu and Al sputtering guns were powered by regulated RF power supplies whereas W was sputtered using dc power. During deposition, rates were controlled by applying constant power to the sources and were monitored with quartz crystal oscillators.

Prior to deposition of the samples, all sputtering guns were thoroughly calibrated for dependence of deposition rates on geometry, sputtering-pressure, and various power-supply parameters. This was done using x-ray interferometric measurements on elemental films and diffraction measurements on multilayers; both made under identical conditions and with less pure targets. Results of these measurements were used to estimate the individual thicknesses of the Cu and Al in the multilayered systems. Samples with two different modulation wavelengths were produced in each multilayer deposition run (with the exception of the W-doped samples and their undoped counterparts) by varying the speed of rotation during deposition of each bilayer. Measurements of the two modulation wavelengths thus obtained provide a second check on the individual material thicknesses. In most cases, the results of these two determinations agree with each other to within 6% or better.

The modulation wavelength and quality of the structure were determined by x-ray diffraction at both small and large angles. Figures 2(a) and 2(b) show typical x-ray diffraction patterns observed in our samples at high and low angles, respectively. Each of the masks on the substrate holders was designed to produce two samples of different geometries side-by-side—one with circular shape for the x-ray measurements and the other one with geometry suitable for the four-probe resistance measurement. Deposition geometry was such that both samples were expected to have identical structural characteristics. X-ray samples were deposited on 0.75 in. dia., 0.25 mm thick sapphire substrates whereas the samples used for resistance measurements were deposited on either sapphire or kapton. The aspect ratio for the resistance samples was approximately 12, and a representation of the sample geometry is given in the insert of Fig. 3. Contacts to the samples were made with either silver paint or Indium solder.

Magnetoresistance was measured with a high precision, four-terminal, ac bridge.[21] Measurements were carried out in a superconducting magnet with a field homogeneity of 0.5% over 1 cm dia. volume. The sample was first mounted perpendicular to the field and magnetoresistance was measured for temperatures from 2.5 K to 20 K, following which the sample was mounted parallel to the field and the steps were repeated. The sample position for the two orientations was the same to within 2 mm. For each temperature, the field was swept from 0 T to about 8 T and back. The field was determined by measuring the current flowing through the superconducting solenoid, with no correction made for the small (about 1.5 mT) residual trapped flux. In each case, a negative field sweep was carried out for at least one temperature to ensure that there was no Hall effect contribution due to sample inhomogeneity. Temperature was measured with a carbon glass thermometer and controlled with a He pressure regulator below 4.2 K and a Lake Shore DRC91C electronic controller above 4.2 K. Typical temperature variation during a field sweep was less than 30 mK, and in the worst case, the relative error in the sample resistance caused by this temperature variation was on the order of 6 ppm or less.

Characteristics of the samples studied are summarized in Table I. They are referred to by numbers 1 through 6 and are arranged in order of increasing conductivity, except for samples 3W and 6W. These two samples are doped with W (less than a monolayer) at the interfaces, but otherwise have the same nominal structure as samples 3 and 6, respectively. Resistivity and modulation wavelength are measured quantities. The individual thicknesses of Cu and Al layers are deduced using the procedures discussed earlier. The average electron concentration (n_{avg}) is calculated as a weighted average of free electron concentrations of bulk Cu and Al, the weights being the respective ratios of individual thickness to modulation wavelength. All other quantities are calculated from n_{avg} and the measured ρ, assuming the

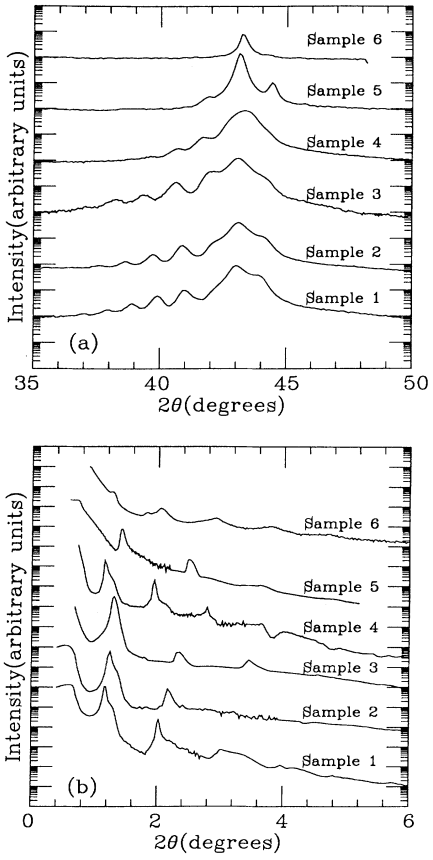

FIG. 2. (a) and (b) are the x-ray diffraction patterns of the samples studied at high and low angles, respectively. Data were taken with Cu $K\alpha$ radiation. These data indicate strong structural anisotropy in these samples, although the width of the diffraction peaks in (a) indicates significant disorder in the growth direction.

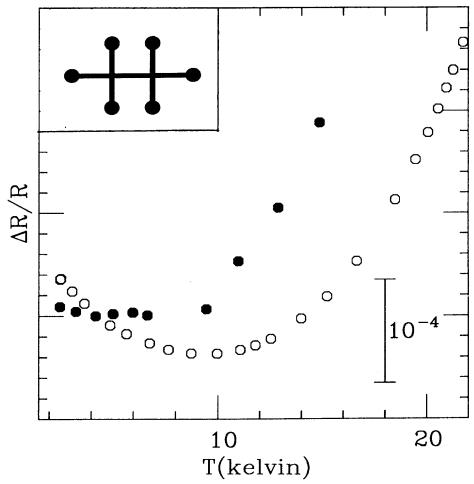

FIG. 3. The normalized change in resistance is plotted as a function of temperature for the highest and the lowest resistivity samples between 2 and 20 K. The open circles represent the sample with the highest resistivity (sample 1) and the solid circles the one with the lowest resistivity (sample 6). In both cases the effects of the quantum corrections to the conductivity are clearly seen in the data below 10 K. The insert shows the geometry of a typical sample used for the magnetoresistance measurements.

free electron gas model.

Some transmission electron microscopy studies on thin film cross sections were performed to obtain a direct visualization of the microstructure in representative samples. The TEM study was done using a Hitachi H-9000 scanning transmission microscope operated at 300 kV. The samples were prepared by embedding pieces of films deposited on kapton in an epoxy resin. Once cured, the piece was cut by ultramicrometry using a diamond knife operated at room temperature. The average thickness of the TEM specimens was around 300 Å.

III. RESULTS AND DISCUSSION

We first wish to consider what may be learned from looking at our data directly, without detailed comparison to theoretical predictions. Transport in metallic multilayers with small modulation wavelengths is similar to that seen in amorphous metals.[22] For instance, Fig. 3 shows the temperature dependence of the resistivity for two representative samples. All other samples show a similar negative temperature coefficient below roughly 10 K, behavior which is qualitatively consistent with the quantum corrections to the conductivity seen in simple metallic glasses such as Mg-Cu.[23] Since WL effects have been studied in amorphous metals for some time now,[24,23] it is reasonable to expect the same effects to be measurable in multilayers. Figures 4–7 show the magnetoresistance data for the Cu/Al multilayers studied. In all cases, the circles represent the data with magnetic field in the plane of the film, the plus signs with field perpendicular to the film, and the solid lines the fits using the WL theory discussed in the Appendix.

Again the data looks qualitatively similar to that seen in experiments on simple metallic glasses. Figure 4 compares data over the entire range of field and temperature with fits to the anisotropic 3D WL theory (see the Appendix) for two representative samples. In this case the fits were performed over only a restricted range of field but the result is extrapolated to cover the entire field range in the figure.[23] Qualitative agreement between the experimental data and the fit is seen on this scale, except at the lowest temperatures or the highest fields. Moreover the data obtained for the two orientations of the magnetic field are almost identical, again except for the highest values of the applied field. This is a strong indication that the dominant contribution to the data comes from three-dimensional weak localization. A further confirmation of this is found in a comparison of data from samples 3 and 6 with that from their tungsten doped counterparts 3W and 6W [Figs. 5(c) compared to 6(a), and 5(f) to 6(b) respectively]. In WL the position of the maximum in the normalized magnetoresistance is related to the strength of the spin-orbit (so) scattering in the sample; this position appearing at larger field for a sample with stronger so scattering. The presence of even a small amount of tungsten is expected to greatly increase so scattering in these samples, so the observations are in keeping with the predictions of WL. The presence of such a small amount of tungsten would be expected to have only a negligible effect on other possible contributions to

TABLE I. Physical parameters for the samples studied. Errors are for resistivity (ρ), ±5%; modulation wavelength (Λ), ±3 Å; individual layer thickness ($d_{Cu,Al}$), ±5 Å. Other parameters are the average electron concentration n_{avg}, the average electron elastic scattering time and mean free path (τ & l_e), the average in-plane electron diffusivity (D), and the cyclotron frequency (ω_c).

Sample	d (Å)	Λ (Å)	d_{Cu}/d_{Al} (Å/Å)	ρ(4.2K) ($\mu\Omega$,cm)	n_{avg} (10^{28}/m^3)	τ (10^{-16}sec)	l_e (Å)	D (cm^2/s)	$\omega_c\tau$ (at 1 T)
1	4185	91	54/37	58.6	12.4	4.9	8.7	15.7	8.6e-5
2	4620	84	43/41	48.8	13.2	5.5	10.1	18.5	9.7e-5
3	3555	79	39/40	35.2	13.4	7.5	13.9	25.5	1.3e-4
4	5225	95	70/25	21.5	11.0	15.0	25.8	44.4	2.6e-4
5	3650	73	62/11	12.3	9.9	29.1	48.6	81.2	5.1e-4
6	3720	93	79/14	9.3	9.9	38.3	64.0	107	6.7e-4
3W	3555	79	39/40	41.9	13.4	6.3	11.6	21.4	1.1e-4
6W	3720	93	79/14	13.3	9.9	26.9	44.9	75.0	4.7e-4

the low temperature magnetoresistance.

Looking at Fig. 5, and comparing the data for the two different field orientations in each case, we note that the normalized magnetoresistance is essentially independent of the field orientation for high resistivity samples but depends strongly on orientation for more conductive samples. The experiments thus give a direct indication of anisotropic transport in these more conductive samples. We show below that the observed anisotropy can be related quantitatively to anisotropy in the electron diffusivity of these materials. Finally, we note that as the more conductive samples are considered the anisotropy first appears in the high-field data, with anisotropy at low fields apparent only for the most conductive samples.

The discrepancies seen in Fig. 4 between the data and the solid line fit to theory appear at high field and low temperature, but are otherwise unlike those normally seen in previous WL studies.[23] We believe these discrepancies to be related to particular features of our multilayered samples. The high-field discrepancy is qualitatively consistent with the presence of a positive quadratic magnetoresistance in addition to the WL contribution. In our subsequent analysis we interpret this as reflecting a conventional $(\omega_c\tau)^2$ contribution, arising from relatively high conductivity material in the middle of the individual layers.[25] We also note that for temperatures below 6.5 K the data falls consistently above theory in the region of the positive MR hump near 100 mT. This behavior is consistent with that seen in systems which undergo a superconducting transition at lower temperatures. It is possible that, particularly in those samples with relatively thick Al layers, a contribution from superconducting fluctuations is being seen for temperatures below 6.5 K. Although we do not see any evidence of superconducting fluctuations in the temperature dependence of these samples down to about 2 K (see Fig. 3), such fluctuations have been known to influence the magnetoresistance at temperatures well above those at which they change the temperature dependence.[23] Measurements at lower temperatures will be needed to determine whether the discrepancies at low temperatures are due to fluctuations, or an inadequacy of the simple anisotropic theory of WL we use to analyze our data. In the absence of such experiments (not to mention the absence of an adequate theory of the MR due to fluctuation conductivity in superconductor/normal metal multilayers) we are unable to analyze the data in this temperature range quantitatively. Consequently we do not include data from temperatures below 6.5 K in our subsequent analysis. However, in all cases the data below 6.5 K is qualitatively consistent with the analysis obtained from the data at 6.5 K and above.

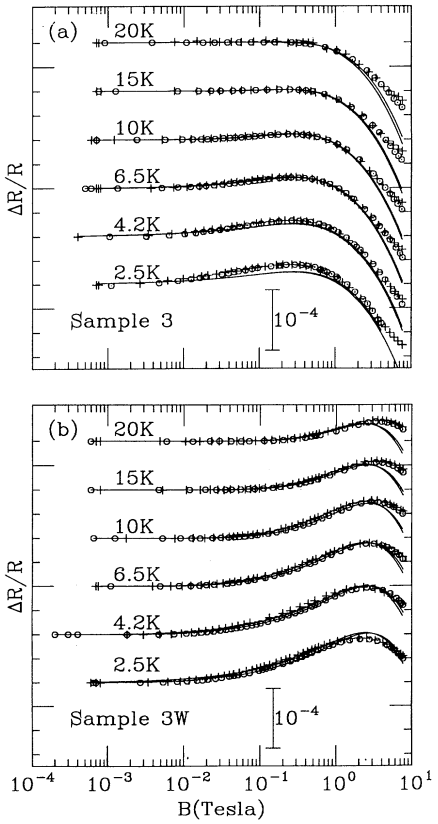

FIG. 4. (a) and (b) are the magnetoresistance data from 2.5 K to 20 K, for a representative sample and its W-doped counterpart, respectively. In both cases the circles represent the situation where the applied field is in the plane of the film, the pluses the field perpendicular to the film, and the solid lines the theoretical fits using Eq. (3.1) with the classical correction term (βB^2) set to zero. Comparison of (a) with (b) shows that the latter has an increased positive magnetoresistance, as expected for weak antilocalization in the presence of the strong spin-orbit scattering introduced by the W doping. The fits are performed over a restricted field range [$B < 2$ T for (a), $B < 4$ T for (b)] and are extrapolated to higher values of the field as described in the text. For clarity only one data point in four appears in the figure.

A more quantitative analysis of the data at higher temperatures is possible through the study of the parameters obtained from fitting a modification of the standard 3D WL theory for anisotropic systems (see the Appendix) to our data. Application of this theory to a multilayer system is valid, provided that the shorter of the length scales, L_ϕ and l_B, is large compared to Λ (which ensures a homogeneous sample) but small compared to the thickness of the film, d (which ensures that the sample will be three dimensional). As can be seen from Table I, the thickness of each of the Cu/Al multilayer films studied is greater than 3500 Å; therefore the condition $d \gg \min(L_\phi, l_B)$ is well satisfied for the values of the magnetic field larger than about 2 mT. Previous structural studies by other workers have shown that the Cu/Al interface is not abrupt and is quite disordered, even in the as-deposited state.[19] Evidence for diffuse interfaces in our samples is evident from Fig. 2(b), where we see only the first few orders of superlattice peaks. This disorder introduces scattering on a length scale much shorter than the modulation wavelength Λ. Therefore, in analyzing our data, we may relax the condition $L_\phi \gg \Lambda$ to a considerable extent, and apply directly the theory discussed in the Appendix.

Equations (A12) and (A14) are expected to describe

our data for the magnetic field oriented perpendicular to, and in the plane of the sample, respectively. As mentioned earlier, in all the samples studied we also see evidence for a positive conventional contribution to the magnetoresistance at high fields. Since the $\omega_c\tau$ values of our samples are much smaller than unity in the entire field range, this conventional contribution is expected to follow $(\omega_c\tau)^2$ behavior[25] and can thus be accounted for by adding a term proportional to B^2 to Eqs. (A12) and (A14). The similarity of these two equations allows us to fit our data to the single expression

$$\left(\frac{\Delta\rho}{\rho}\right) = \alpha\,\frac{e^2}{2\pi^2\hbar}\sqrt{\frac{eB}{\hbar}}\left[\frac{1}{2}\,f_3\left(\frac{B}{B_\phi}\right) - \frac{3}{2}\,f_3\left(\frac{B}{B_\phi + 4/3B_{so}}\right)\right] + \beta\,B^2\,, \tag{3.1}$$

where the prefactors involving the components of diffusivity [in Eqs. (A12) and (A14)] have been absorbed in the quantity α, and all four of the quantities α, B_{so}, B_ϕ, and β are now dependent on the orientation of the applied magnetic field. These quantities are related to the components of the electron diffusivity tensor in the following way:

$$\frac{D_{xy}}{D_z} = \left(\frac{[B_{so}]_\parallel}{[B_{so}]_\perp}\right)^2 = \left(\frac{[B_\phi]_\parallel}{[B_\phi]_\perp}\right)^2 . \tag{3.2}$$

and

$$\frac{D_{xy}}{D_z} = \left(\frac{[\alpha]_\perp}{[\alpha]_\parallel}\right)^2 = \left(\frac{[\beta]_\perp}{[\beta]_\parallel}\right)^{1/2} . \tag{3.3}$$

Here, the subscripts $\parallel$ and $\perp$ indicate the orientation of the magnetic field (parallel and perpendicular to the plane of the film, respectively), D_{xy} is the diffusivity for electrons moving in the sample plane, and D_z is the diffusivity for electrons moving along the growth direction.

While fitting to our data using Eq. (3.1), we treat the quantities α, B_{so}, B_ϕ, and β as adjustable parameters, and Eqs. (3.2) and (3.3) are then used to obtain a measure of the anisotropy ratio $\delta = D_{xy}/D_z$. The result in the second part of Eq. (3.3) comes from the linear de-

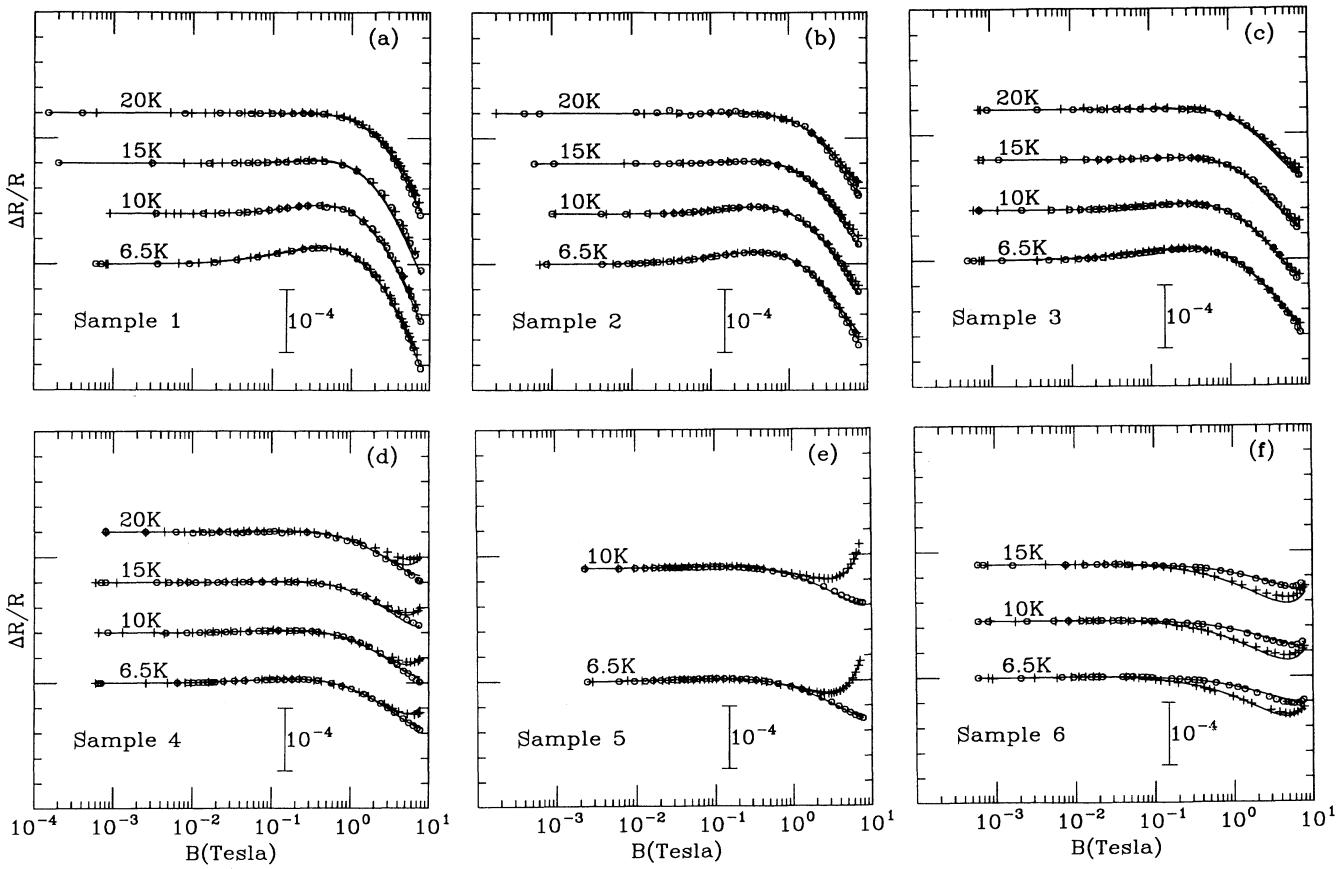

FIG. 5. (a) to (f) are the magnetoresistance data for samples 1 to 6, respectively. In all cases the data for temperatures below 6.5 K are excluded. The data have been decimated for clarity, as was the case in Fig. 4. The circles represent the data with magnetic field in the plane of the film, the pluses the field perpendicular to the film, and the lines the fits, with the classical correction (βB^2) included. Comparison of 5(c) and 4(a) shows that including the classical correction improves the fits at high fields.

pendence of the diffusivity on the elastic scattering time ($D = v_F^2\tau/3$), and the quadratic dependence of the conventional magnetoresistance on τ. The equations in (3.2) are valid if we assume that the inelastic and spin-orbit scattering rates (τ_{so}^{-1} and τ_ϕ^{-1}) themselves are isotropic, even when the elastic scattering rate (τ^{-1}) is not. Previous work[26] has shown that τ_ϕ^{-1} is relatively independent of the strength of disorder (i.e., τ^{-1}) and hence this assumption should be valid for the ratio $[B_\phi]_\parallel/[B_\phi]_\perp$. The disorder dependence of τ_{so}^{-1} has not been studied previously; however, we obtain a rough estimate for this dependence, in the discussion below, using the values of B_{so} obtained from the fits, and find that it is similarly insensitive to τ. Note that since α, B_{so}, and β are all temperature independent, fitting to data at different temperatures simultaneously allows us to keep the effective number of adjustable parameters per temperature to less than two for most of the data. An unfortunate exception to this is found in the case of sample 5, which was destroyed before we were able to collect data at 15 and 20 K. We would like to point out, however, that the B_{so} value, in particular, is determined primarily by the data below 15 K, so the analysis of the data for sample 5 does not suffer too much from this loss.

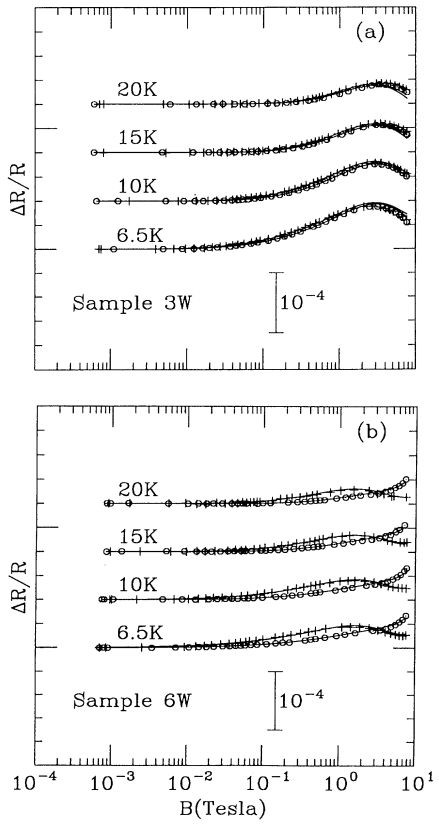

FIG. 6. The magnetoresistance data for the W-doped samples. The data for temperatures below 6.5 K are excluded. The circles are the data with the field in the plane of the film, the pluses the field perpendicular to the film, and the lines the theoretical fits with the classical correction (βB^2) included.

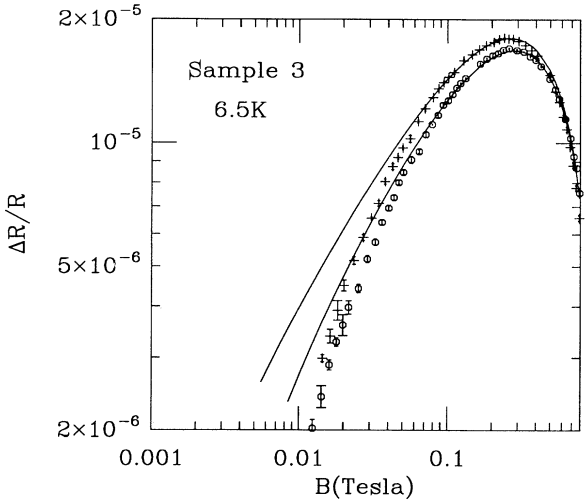

FIG. 7. Representative low-field magnetoresistance data plotted on a log-log scale. The circles represent the data with the field in the plane of the film, the pluses the field perpendicular to the film, and the lines are the theoretical fits. For both the field orientations the data are seen to deviate from the theory as one goes towards smaller values of the field. This suggests that the simple anisotropic 3D WL theory used here may not be completely accurate at long length scales. Residual contributions from superconducting fluctuations or flux cancellation effects may be responsible for the observed discrepancies.

We begin our quantitative analysis with a sample of intermediate resistivity (sample 3 $\rho = 35.2\ \mu\Omega$ cm). Figure 4(a) shows the data for this sample for temperatures from 2.5 K to 20 K, and Fig. 4(b) for the corresponding W doped sample. The theoretical fits in both these figures are obtained by setting the conventional contribution in Eq. (3.1) to zero. For each orientation of the field, the values of B_{so} and β are adjusted for the data from 2.5 K to 20 K simultaneously, whereas, individual B_ϕ values are adjusted for each temperature. For Fig. 4(a), only data up to 2 T is used for the fit, since beyond about 2.5 T the magnetic length(l_B) becomes comparable to the modulation wavelength of this sample. For Fig. 4(b) however, data up to 4 T is used. This is because, in order to get a meaningful value of B_{so}, the spin-orbit scattering peak must be included in the fitting range. In both cases the fit is then extrapolated to higher values of the field. As mentioned above, our quantitative analysis will concentrate on the the temperatures from 6.5 K to 20 K. Over this range the fits in Fig. 4 agree well with the data on the displayed scale except at high fields, where the extrapolated theory curves are seen to lie below the experimental data.

In subsequent figures the data for 2.5 K and 4.2 K are excluded, and the conventional contribution is included in the fitting procedure. For each sample, we first estimate the value of the field (B_Λ) at which l_B equals the modulation wavelength. We fit to data up to this value of B, for all temperatures above 4.2 K using the anisotropic WL theory with single values for α and B_{so} and one value of B_ϕ for each temperature. This procedure yields values

for the adjusted parameters α, B_{so}, and $B_\phi(T)$'s with minimal interference from the classical term, which is only important at larger fields. This cannot be done for samples 6W and 3W, since for these samples accurate measurements of B_{so} require fitting to data up to field values considerably greater than B_Λ. Next, using these values for α, B_{so}, $B_\phi(T)$'s, and fitting to the entire field range, we adjust β for temperatures from 6.5 K to 20 K simultaneously. Comparison of Fig. 4(a) with Fig. 5(c) [or 4(b) with 6(a)] shows that inclusion of the conventional contribution improves the agreement between theory and data at high fields. The uncertainties listed for the optimal values of the fitting parameters in Table II indicate the range of values obtained for these parameters from variations of the above procedure, such as changing the range over which the initial WL fit was performed.

In principle, Eqs. (3.2) and (3.3) provide us with four different avenues to obtain the anisotropy ratio, $\delta = (D_{xy}/D_z)$, using the parameters obtained from fitting to our data. Our results indicate that the anisotropy ratios obtained from α, B_{so}, and β are reasonably consistent with one another. On the other hand, consistent agreement between these and the anisotropy ratios obtained from the B_ϕ values at different temperatures seems to be an exception rather than the rule.

It is not surprising, however, that the ratio of the B_ϕ values should turn out to be the least well defined of the four ratios discussed in Eqs. (3.2) and (3.3). This is the only one of the four which is not based on an average over several temperatures, and previous work on WL in 3D systems typically found the scatter in B_ϕ values to be rather large.[23,27] In the present study the B_ϕ values are often small enough to be comparable to our uncertainty in the field measurement, and indeed small enough to make L_ϕ comparable to the thickness of the film. Moreover, a close look at the low field region for some typical data from Fig. 5 reveals small but systematic departures from the theoretical prediction (see Fig. 7), casting further suspicion on the reliability of the values of B_ϕ obtained from the fit. Such deviations at low fields could be caused by superconducting fluctuations, sample geometric constraints (expected when L_ϕ is comparable to d), or perhaps even a flux cancellation effect such as is seen in 2D WL measurements on "clean" thin films.[28] Further experiments on other systems will be necessary to determine the importance of each of these contributions to the observed discrepancies. Given these difficulties in obtaining reliable numbers for the ratio $[B_\phi]_\parallel/[B_\phi]_\perp$, we concentrate below on the three other determinations of the anisotropy ratio. It is worth emphasizing at this point, however, that on the scale of Fig. 7 anisotropy is again seen directly in the data; as a different magnitude and position for the spin-orbit maximum in the MR in the two different field orientations. Thus, even in a sample with small anisotropy such as 3, the anisotropy is revealed directly in the data, independent of the details of any complicated fitting procedure.

TABLE II. Values of the characteristic spin-orbit field obtained from the fits of an anisotropic 3D WL theory to our data for parallel ($\parallel$) and perpendicular ($\perp$) orientations of the applied field. As described in the text, τ is the elastic scattering time.

Sample	$[B_{so}]_\parallel$ (mT)	$[B_{so}]_\perp$ (mT)	$[B_{so}]_\parallel^2/[B_{so}]_\perp^2$	$\tau[B_{so}]_\parallel$ (10^{-17} T sec)
1	114 ± 6	113 ± 6	1.02 ± 0.05	5.6
2	107 ± 2	103 ± 3	1.08 ± 0.05	5.9
3	80 ± 0.6	75 ± 0.5	1.14 ± 0.03	6.0
4	50 ± 0.5	47 ± 0.3	1.13 ± 0.1	7.5
5	31 ± 2	25 ± 3	1.5 ± 0.2	9.0
6	7.3 ± 1	4.5 ± 2	2.6 ± 1.0	2.8
3W	810 ± 60	730 ± 100	1.23 ± 0.05	50
6W	750 ± 100	400 ± 70	3.5 ± 1.0	200

Values of B_{so}, α, and β obtained from the fits, for each orientation of the field, are plotted against the sample resistivity in Fig. 8. The ratios which enter into Eqs. (3.2) and (3.3) are plotted against the sample resistivity in Fig. 9. We notice that, particularly when considering the ratio of B_{so} values, small anisotropies are revealed even in cases where the eye cannot see it immediately from the data in Figs. 5(a)–5(h). In carrying out the fitting procedure for various field ranges, we noticed that the scatter in the B_{so} values is very small. Furthermore, when variations in the fitting procedure are considered, the values of $B_{so\parallel}$ and $B_{so\perp}$ are found to be correlated making the uncertainty in the ratio somewhat smaller than the sum of the relative uncertainties for each direction in most cases. The scatter in the values of α and β obtained from the fits is somewhat larger than that of B_{so}. For α this is expected because this parameter is the most sensitive to drifts in the bridge, or shifts in its gain. On the other hand, the accuracy of the β value is limited since it depends on an extrapolation of the expression for the WL contribution to high fields, where other phenomena (such as electron-electron interactions) may interfere with the measurement. The ratio $\delta_{B_{so}} = [B_{so}]_\parallel^2/[B_{so}]_\perp^2$ thus appears to be the most well defined of the four listed in Eqs. (3.2) and (3.3). However, as noted above, the question of whether this ratio may be directly related to the ratio of the electron diffusivities must still be addressed.

The ratio of spin-orbit fields is tied directly to the ratio of in-plane and out-of-plane diffusivities only if the spin-orbit scattering rate itself is isotropic. In principle, anisotropy in this rate could arise from either a layered distribution of spin-orbit scattering sites (such as the W atoms in our doped samples), or through a dependence of the spin-orbit scattering rate on the elastic scattering rate τ^{-1} if the latter is anisotropic. The calculation of spin-orbit scattering rates is a difficult problem even in a homogeneous system, and hence performing such calculations for these multilayers is beyond the scope of the present work. However, in Table II we list a quantity which is roughly proportional to this rate, $[B_{so}]_\parallel\tau \propto {\tau_{so}}^{-1}$. We note that, particularly for those systems in which the Cu and Al concentrations are approximately equal (i.e., samples 1 through 4), this quantity varies by only 30%, even though τ^{-1} varies by a factor of three! While it should be remembered that the values listed for τ in Table I are only rough estimates of a quantity averaged over an inhomogeneous system, and

it is possible that there may be some fortuitous cancellation of the dependence of τ_{so}^{-1} on τ^{-1} and on composition, this observation is a strong indication that τ_{so}^{-1} is insensitive to τ^{-1} in our samples. The extreme value of the ratio in sample 6W no doubt reflects anisotropy in the spin-orbit scattering rate itself due to the layered distribution of strong spin-orbit scattering centers in this sample. Hence for this sample $\delta_{B_{so}}$ undoubtedly overestimates the diffusion anisotropy to a considerable degree. In sample 3W the layers of tungsten atoms are not so well separated as they are in sample 6W, and hence the spin-orbit scattering rate itself appears to be less anisotropic

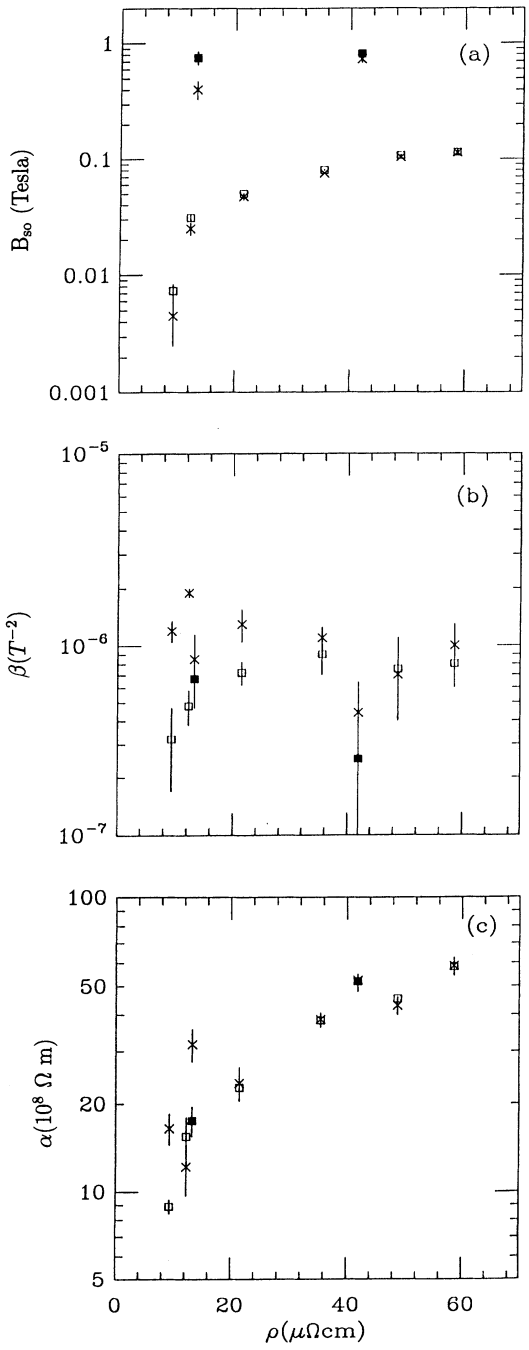

FIG. 8. The B_{so}, α, and β values obtained from the fits, for both the field orientations, are plotted against the measured sample resistivity. The squares denote the values for the case of the magnetic field in the plane of the film and the crosses the case with the field perpendicular to the film. The solid squares distinguish the W-doped samples from the undoped ones.

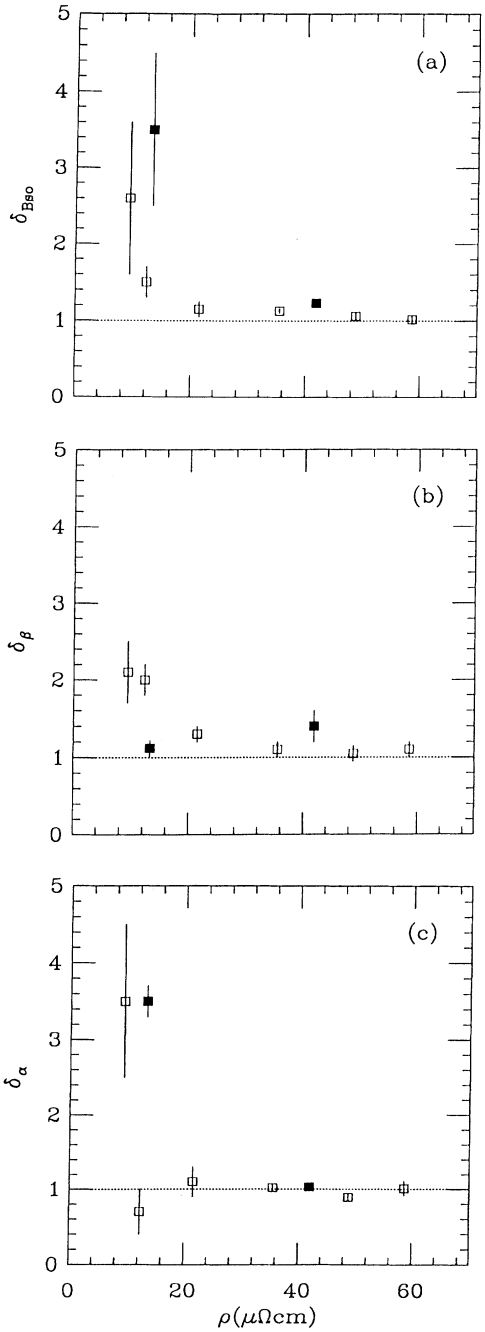

FIG. 9. The ratios $\delta_{Bso} = [B_{so}]_\parallel^2/[B_{so}]_\perp^2$, $\delta_\alpha = [\alpha]_\perp^2/[\alpha]_\parallel^2$, and $\delta_\beta = [\beta]_\perp^{1/2}/[\beta]_\parallel^{1/2}$ obtained from the fits are plotted against the measured sample resistivity. The solid squares distinguish the W-doped samples from the undoped ones.

in this case. On the other hand, the rate is likely to be more anisotropic in this sample than in any of the undoped samples, since the dominant sites (the W atoms) are arranged in layers. The centers responsible for spin-orbit scattering in the undoped samples are not known, but they are most certainly more uniformly distributed than are the W atoms in sample 3W. Given the small difference between the values of $\delta_{B_{so}}$ in samples 3W and 3, an assumption that anisotropy in τ_{so}^{-1} makes only a negligible contribution to $\delta_{B_{so}}$ for the undoped samples is certainly reasonable. Thus we believe that the ratio $[B_{so}]_{\|}^2/[B_{so}]_{\perp}^2$ represents our best estimate for the diffusion anisotropy in our samples, at least those which are not doped with tungsten. Based on the above analysis, this ratio overestimates the diffusion anisotropy by less than 20%, even for the largest anisotropy we observe (sample 6), and the uncertainty in the ratio itself is substantially larger than this.

We now turn our discussion to the question of whether the anisotropy we observe in the above MR experiments is consistent with what might be expected on the basis of the other information we have regarding the structure of our samples. Trivedi and Ashcroft[6] have used a semiclassical approach to consider the anisotropy of transport expected in a multilayer where disorder was modeled by scattering centers restricted within slabs which are periodically repeated in an otherwise clean host metal. In the "thick slab" limit of their calculation, when the thickness of the slab of disorder approaches the modulation wavelength, the resistivity becomes isotropic. At the other extreme, anisotropies as large as $\delta = 2$ were seen in cases in which the slab thickness was roughly 20% of the repeat distance.

We attempt to make contact with this model by analyzing the sample to sample variation in resistivity seen in Table I. Note that samples in which the individual thicknesses of Cu and Al layers are comparable have higher resistivities than the ones in which the Al layer is much thinner than the Cu layer. This resistivity variation can be explained using a simple model in which a multilayer is made of alternating layers of pure Cu and pure Al with a "disordered" phase (characterized by thickness t and resistivity ρ_t) occupying a part of each layer near the interface, and assuming that the layers act as independent resistors, connected in parallel.[29] We treat the Cu and Al layers as free electron metals with bulk values for k_F and a mean free path limited by scattering at the boundaries between the "pure" layer and the disordered layers surrounding it. In applying such a model to our samples, we notice that for those samples where the Al layer thickness is much smaller than the Cu layer thickness, and any reasonable value of ρ_t, the disorder is almost entirely confined to the Al layer, leaving the thick Cu layer almost completely clean. In these samples this distribution of disorder is not surprising since the Al layers would be expected to be more susceptible to inclusion of oxygen and other impurities from the residual gases in the chamber. The resulting stratified nature of the disorder accounts for the low resistivity of these samples, and leads one to expect anisotropic electron transport. On the other hand, for the samples in which the Cu and Al layer thicknesses are comparable, the extent of the disordered region required to explain their higher resistivities is on the order of the modulation wavelength, which would suggest more isotropic transport for these cases.

The thickness predicted by this simple model for the disordered layer, expressed as a fraction of the modulation wavelength, is shown in Fig. 10 as a function of sample resistivity. This figure indicates that in the sample which shows the greatest anisotropy (sample 6, $\delta = 2.6 \pm 1$), the disordered layer thickness is between 15% and 30% of the modulation wavelength. This is similar to the calculations of Trivedi and Ashcroft ($\delta \approx 2$ at $t/\Lambda = 0.2$) in which parameters were chosen to model a layered distribution of Si scattering centers within an Al matrix.

The x-ray scattering results shown in Fig. 2 also support the above model for the structure of these multilayers. The absence of a distinct peak near 38.5° [Al (111)] in the envelope function of the high angle reflections in Fig. 2(a) argues in favor of a large amount of structural disorder within the Al layers. This is particularly true for the most conductive sample which shows a rather sharp diffraction peak at high angle but no coherent scattering near the (111) peak of Al. In sample 6 the disappearance of the satellite lines indicates that the Al layers have lost coherence with the Cu layers, and possibly even become discontinuous [suggested by the sharpness of the peak at Cu (111)]. It is somewhat surprising that samples 1 through 4 exhibit as many satellite reflections at high angle as they do, given the disorder which is evident from both the widths of the reflections, and the size of these samples' resistivities. It is important to remember, however, that the widths of these reflections indicate the quality of the superlattice in the growth direction, whereas the resistivity is sensitive to departures from perfect periodicity within the bilayers themselves. The observed behavior could indicate a large concentra-

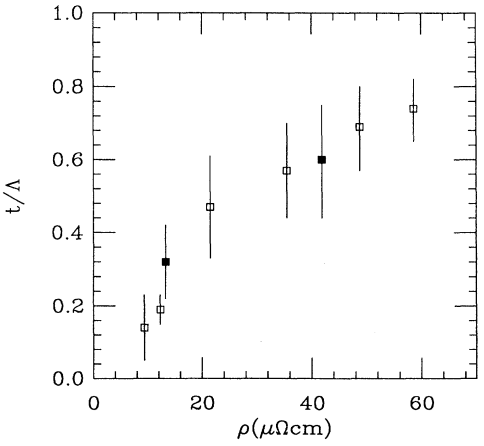

FIG. 10. The ratio of the thickness of the disordered phase to the modulation wavelength (t/Λ), calculated using a simple transport model for the multilayer as described in the text, is plotted as a function of the measured sample resistivity. The solid squares distinguish the W-doped samples from the undoped ones.

tion of strain relieving defects within the bilayers for samples 1 through 4. Such disorder would lead to a large resistivity and could reduce the coherence in the growth direction to a degree necessary to widen the satellite reflections, while maintaining enough coherence to produce satellite reflections in the first place.[30]

The above discussion is supported, at least qualitatively, by the structures seen in the cross sectional TEM images shown in Fig. 11. This figure shows images at two different magnifications for samples 1 and 6. The samples were prepared for TEM by ultramicrotome sectioning which makes quantitative analysis of the images somewhat doubtful due to the large distortions of the sample which may result from such treatment. In particular, it is not possible to clearly identify the manner in which disorder is distributed within the bilayers. The TEM is consistent with Fig. 2(b) in that both samples show evidence of layering, but without a well ordered superlattice structure. However, in comparing 11(a) with 11(b), sample 6 indeed appears to be less homogeneous than sample 1. Thus it is not surprising that sample 6 displays more anisotropy in the transport. At higher magnification, sample 1 reveals lattice fringes throughout the multilayer [Fig. 11(c)], and it is possible to measure the fringe spacing for both layers. The values obtained (around 2.1 and 2.3 Å) indicate that these fringes correspond to the (111) planes of Cu and Al, suggesting some epitaxial growth in this case. There is substantial lattice mismatch (12%) between Cu and Al and hence a large concentration of misfit dislocations can be expected within the layers of this sample. On the other hand, sample 6 shows no such long range coherence [Fig. 11(d)]. For this sample different regions of the sample exhibit fringe patterns indicative of different crystal orientations. This accounts for the absence of satellites in the high angle x-ray diffraction measurements, and the associated reduced defect density can account for the lower resistivity.

IV. CONCLUSIONS

We have measured the magnetoresistance in a series of Cu/Al multilayers for two different orientations of the

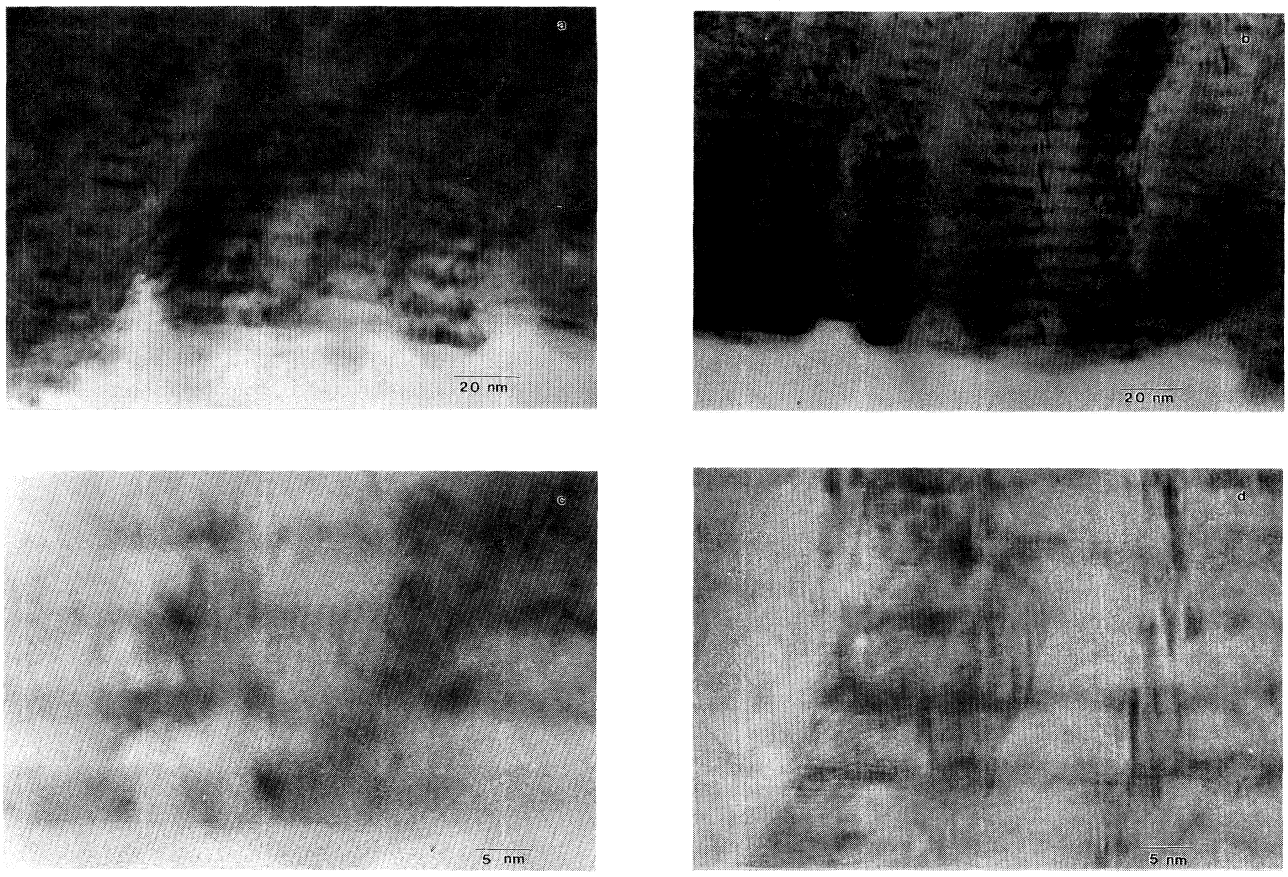

FIG. 11. Cross sectional TEM images of sample 1 [(a) and (c)] and sample 6 [(b) and (d)]. At lower magnification [(a) and (b)] we see that the structure in sample 6 is more stratified than is the case with sample 1, as expected for a sample showing greater anisotropy in its transport properties. In the higher magnification images greater coherence at the atomic level in sample 1 [figure (c)] is evident in the appearance of lattice fringes throughout the sample. In contrast to this, the lattice fringes observed in sample 6 [figure (d)] indicate some variation in the orientation of the crystals, revealing a lack of orientational coherence in this sample. This is consistent with the high angle x-ray diffraction results in 2(a).

magnetic field. The multilayers considered exhibit a relatively large amount of disorder within the bilayers, leading to relatively high resistivities and weak localization effects. The dominant contribution to the magnetoresistance comes from weak localization, with another contribution from the conventional $(\omega_c\tau)^2$ magnetoresistance visible at high fields. We have shown that it is possible to analyze these data in such a way as to provide a measurement of the anisotropy of electron transport in metallic multilayers. As one looks at samples with thinner Al layers, the disorder becomes more concentrated in the Al layers leaving relatively clean copper layers. This stratified arrangement of disorder leads to a measurable anisotropy in the electron diffusivity for these materials (D_{xy}/D_z as large as 2.6 ± 1.0), and the size of this anisotropy is similar to that predicted by Trivedi and Ashcroft.[6] These results indicate that magnetoresistance measurements offer a tool with which the anisotropy of the electron diffusivity in multilayers may be measured. This, in turn, may provide a probe of the way in which disorder is distributed in such materials. However, additional experiments on other samples will be needed in order to establish the reliability of this probe. Such tests are currently under way using Cu/Si multilayers, where the disorder and spin-orbit scattering rates are such that it may be possible to obtain reliable values for both B_{so} and B_ϕ, thereby providing a consistency check on the various assumptions underlying the method.

ACKNOWLEDGMENTS

This work was supported by the NSF under Contract No. DMR89-18139. The authors would like to acknowledge fruitful discussions with John Carini, Ulrich Wulf, and Allan H. MacDonald.

APPENDIX

1. Basic WL theory

Using Green function techniques and Kubo's linear response theory, one can calculate the quantum interference induced correction to Boltzmann conductivity due to WL by solving the so-called maximally crossed diagrams.[8] Typically, one first calculates the frequency (ω) dependent conductivity correction in the limit $\omega\to 0$ and then $-i\omega$ is replaced by $1/\tau_\phi$ to take into account the loss of phase coherence for the time scales $\gg\tau$, where τ is elastic scattering time. The result for frequency dependent correction in homogeneous, isotropic, 3D systems can be conveniently written as

$$\delta\sigma(\omega)_{\rm WL} = -\frac{4\pi\nu(\epsilon_F)\tau}{\hbar}\frac{e^2}{\pi\hbar}D\tau\int\frac{d^3q}{(2\pi)^3}\Gamma(\mathbf{q},\omega). \quad \text{(A1)}$$

where, the quantity $\Gamma(\mathbf{q},\omega)$ is the so-called Cooperon, D is the electron diffusion constant, and $\nu(\epsilon_F)$ is the density of states at Fermi energy.

In the presence of spin-orbit scattering characterized by spin-orbit scattering time $\tau_{\rm so}$, Γ has the following structure:[31]

$$\Gamma(\mathbf{q},\omega) = \frac{\hbar}{2\pi\nu(\epsilon_F)\tau}\left[\frac{3}{2}\frac{1}{Dq^2\tau - i\omega\tau + \frac{4\tau}{3\tau_{\rm so}}} - \frac{1}{2}\frac{1}{Dq^2\tau - i\omega\tau}\right]. \quad \text{(A2)}$$

The expressions (A1) and (A2) may be used to calculate the magnetoresistance[32] for the magnetic fields satisfying $\omega_c\tau\ll 1$ and $l_B\gg l_e$, simply by making the replacement

$$Dq^2 \longrightarrow 4Dl_B{}^{-2}(N+1/2) + Dq_\parallel^2 \quad \text{(A3)}$$

and summing over N. Here, $\omega_c = eB/m$ is the cyclotron frequency, $l_B = \sqrt{\hbar/4eB}$ is the magnetic length, l_e is the elastic mean free path, N is the quantum number representing the Landau level, and $q_\parallel$ is the component of $\mathbf{q}$ in the direction of magnetic field. Thus Γ, in the presence of spin-orbit scattering and external magnetic field B, is given by

$$\Gamma(\mathbf{q},\omega,B) = \frac{\hbar}{2\pi\nu(\epsilon_F)\tau}\sum_N\left[\frac{3}{2}\frac{1}{4Dl_B{}^{-2}(N+1/2)\tau + Dq_\parallel{}^2\tau - i\omega\tau + \frac{4\tau}{3\tau_{\rm so}}} - \frac{1}{2}\frac{1}{4Dl_B{}^{-2}(N+1/2)\tau + Dq_\parallel{}^2\tau - i\omega\tau}\right]. \quad \text{(A4)}$$

Substituting Γ from Eq. (A4) into Eq. (A1), performing the integral, and replacing $-i\omega$ by $1/\tau_\phi$ yields the final result for magnetoconductivity due to WL. It is more convenient, however, to express it as a normalized change in resistivity; since that is the quantity usually measured in experiments. We present here the result valid for systems with high electron diffusivity ($D > 2$ cm^2/sec) and no magnetic impurities:[9,20,33]

$$\left[\frac{\delta\rho(B)}{\rho}\right]_{WL} = \rho\frac{e^2}{2\pi^2\hbar}\sqrt{\frac{eB}{\hbar}}\left[\frac{1}{2}f_3\left(\frac{B}{B_\phi}\right) - \frac{3}{2}f_3\left(\frac{B}{B_\phi + 4/3B_{\rm so}}\right)\right]. \quad \text{(A5)}$$

B_ϕ and B_{so} are the dephasing field and the spin-orbit scattering field, respectively, and are defined by

$$B_{\phi,{\rm so}} = \frac{\hbar}{4eD\tau_{\phi,{\rm so}}}. \quad \text{(A6)}$$

The function f_3 is given by

$$f_3(x) = \sum_{N=0}^{\infty} \left[2\left(N+1+\frac{1}{x}\right)^{1/2} - 2\left(N+\frac{1}{x}\right)^{1/2} - \left(N+\frac{1}{2}+\frac{1}{x}\right)^{-1/2} \right] . \tag{A7}$$

2. WL in multilayered systems

So far we have talked only about isotropic systems. Now, we discuss the modifications necessary in the above formalism, in order to apply it to a multilayered system, which is inherently anisotropic. The superlattice WL theory of Szott, Jodrezejek, and Kirk[16] has been developed for such a situation. However, this theory considered only one direction for the applied field, and its major difference from a simple anisotropic medium approach was to be found in the prefactor, α [see Eq. (3.1)], which was found to depend on the miniband width. Given the amount of disorder in our multilayers, the miniband width is not something that we can easily estimate. Therefore in analyzing our data we have followed the treatment by Bhatt, Wölfle, and Ramakrishnan,[34] who have solved the problem for systems which are homogeneous on the length scale of WL, but have an anisotropy on the microscopic scale which may be completely described by anisotropic diffusion tensor $D_{\mu\nu}$. Their result (with no external magnetic field or spin-orbit scattering) for $(\delta\sigma_{\mu\mu})_{\rm WL}$ is the same as Eq. (A1), except that the diffusion constant D in the prefactor is replaced by $D_{\mu\mu}$ and the Dq^2 term in Γ is replaced by $\sum_\mu D_{\mu\mu}q_\mu^2$. Their result for 3D systems can be extended to include the effects of spin-orbit scattering in the same way as A1, and when an external magnetic field is present, once again, one has to invoke the Landau quantization. Here, appropriate replacement for Dq^2 is

$$Dq^2 \longrightarrow 4D_\perp l_B^{-2}(N+1/2) + D_\parallel q_\parallel^2 , \tag{A8}$$

where $D_\parallel$ is the component of diffusivity in the field direction and $D_\perp$ is the effective diffusivity in the plane perpendicular to the field. Hence, Γ for anisotropic systems is

$$\Gamma_a(\mathbf{q},\omega,B) = \frac{\hbar}{2\pi\nu(\epsilon_F)\tau} \sum_N \left[\frac{3}{2} \frac{1}{4D_\perp {l_B}^{-2}(N+1/2)\tau + D_\parallel {q_\parallel}^2\tau - i\omega\tau + \frac{4\tau}{3\tau_{\rm so}}} - \frac{1}{2} \frac{1}{4D_\perp {l_B}^{-2}(N+1/2)\tau + D_\parallel {q_\parallel}^2\tau - i\omega\tau} \right] \tag{A9}$$

and the change in conductivity due to WL is given by

$$\delta\sigma_{\mu\mu}(\omega)_{WL} = -\frac{4\pi\nu(\epsilon_F)\tau}{\hbar}\frac{e^2}{\pi\hbar} D_{\mu\mu}\tau \int \frac{d^3q}{(2\pi)^3}\Gamma_a(\mathbf{q},\omega,B). \tag{A10}$$

Note that Eqs. (A8) and (A9) have the same form as Eqs. (A1) and (A4), respectively, except that the diffusion constant D is replaced by components of diffusivity tensor $D_\perp$ and $D_\parallel$. However, in this case, since $D_\perp$ and $D_\parallel$ depend upon the orientation of magnetic field with respect to the sample, Γ and $\delta\sigma$ are functions of field orientation as well.

The foregoing analysis can be applied to a multilayer system provided L_ϕ (the dephasing length) and l_B (the magnetic length) satisfy the condition,

$$d \gg \min(L_\phi, l_B) \gg \Lambda , \tag{A11}$$

where d is the smallest of the physical dimensions of the sample and Λ is the modulation wavelength of the multilayer structure. The first inequality ensures the three-dimensionality of the sample and the second one implies homogeneity on the length scale of WL.

The final result is once again obtained by substituting Γ from Eq. (A9) into Eq. (A10), integrating and replacing $-i\omega$ by $1/\tau_\phi$. Our measurements involve two different orientations of the magnetic field—in the plane of and perpendicular to the multilayer film. We present here the results of the calculation for these two cases. In our setup, the current direction is held fixed (in the plane of the film in both cases) and the quantity measured is always $[\delta\rho_{xx}(B)/\rho_{xx}]$. However, in the following we have dropped the subscript on ρ to simplify the notation. Note also that we have written the diffusivity tensor in terms of its component perpendicular to the film plane (D_z) and a component in plane (D_{xy}).

Case 1: B perpendicular to the film. In this case the component of D along the field direction is D_z, the effective diffusivity in the plane perpendicular to the field is D_{xy}, and the normalized change in resistivity is given by

$$\left[\frac{\delta\rho(B\perp\text{film})}{\rho}\right]_{\rm WL} = \left(\frac{D_{xy}}{D_z}\right)^{1/2} \rho\frac{e^2}{2\pi^2\hbar}\sqrt{\frac{eB}{\hbar}} \left[\frac{1}{2} f_3\left(\frac{B}{B_\phi}\right) - \frac{3}{2} f_3\left(\frac{B}{B_\phi + 4/3B_{\rm so}}\right)\right] \tag{A12}$$

with

$$B_{\phi,\mathrm{so}} = \frac{\hbar}{4eD_{xy}\tau_{\phi,\mathrm{so}}} . \tag{A13}$$

Case 2: B in the plane of the film. In this case the component of D along the field direction is D_{xy}, the effective diffusivity in the plane perpendicular to the field is $\sqrt{D_{xy}D_z}$, and the normalized change in resistivity is given by

$$\left[\frac{\delta\rho(B \parallel \text{film})}{\rho}\right]_{\mathrm{WL}} = \left(\frac{D_{xy}}{D_z}\right)^{1/4} \rho \frac{e^2}{2\pi^2\hbar} \sqrt{\frac{eB}{\hbar}} \left[\frac{1}{2} f_3\left(\frac{B}{B_\phi}\right) - \frac{3}{2} f_3\left(\frac{B}{B_\phi + 4/3B_{\mathrm{so}}}\right)\right] \tag{A14}$$

with

$$B_{\phi,\mathrm{so}} = \frac{\hbar}{4e(D_{xy}D_z)^{1/2}\tau_{\phi,\mathrm{so}}} \tag{A15}$$

Expressions (A14) and (A15) have the same form as (A5) except for the prefactors involving the ratios of components of diffusivity and the definitions of B_ϕ and B_{so} given by (A13) and (A15). In summary, the main consequence of the anisotropy is a dependence of field scales for the magnetoresistance, B_ϕ, and B_{so}, on the orientation of magnetic field with respect to the sample film. A similar dependence of the prefactor in front of the right-hand sides of Eqs. (A12) and (A14) on the orientation of the field is also seen.

As noted previously, the use of a full superlattice theory for the WL magnetoresistance in multilayers is expected to give results very similar to these, but with prefactors which include factors other than the components of the diffusion tensor. Measurements on multilayers whose quality is superior to those studied here will be needed to discern the effects associated with the miniband structure which are responsible for these differences.

[1] For a comprehensive review of the work done on metallic multilayers up to 1989 the reader is referred to B.Y. Jin and J.B. Ketterson, Adv. Phys. **38**, 189 (1989).

[2] E. Spiller, in *Low Energy X-Ray Diagnostics–1981*, edited by D.T. Attwood and B.L. Henke (AIP, New York 1981), p. 124.

[3] *Synthetically Modulated Structures*, edited by L.L. Chang and B.C. Giessen (Academic, New York, 1985).

[4] C.-X. Chen, Appl. Phys. A **42**, 145 (1987).

[5] R. Dimmich, J. Phys. F **15**, 2477 (1985).

[6] N. Trivedi and N. Ashcroft, Phy. Rev. B **35**, 6084 (1987).

[7] J.M. Slaughter, W.P. Pratt Jr., and P.A. Schroeder, Rev. Sci. Instrum. **60**, 127 (1989).

[8] G. Bergmann, Phys. Rep. **107**, 1 (1984).

[9] B.L. Altshuler, A.G. Aronov, in *Electron-Electron Interaction in Disordered Systems* (edited by A.L. Efros and M. Pollak (North-Holland, Amsterdam, 1985).

[10] R.P. Peters, G. Bergmann, and R.M. Mueller, Phys. Rev. Lett. **58**, 1964 (1987).

[11] P.M. Menz, R.G. Wheeler, C.T. Foxon, and J.J. Harris, Appl. Phys. Lett. **50**, 603 (1987).

[12] D.V. Baxter, R. Richter, and J.O. Strom-Olsen, Phys. Rev. B **35**, 4819 (1987).

[13] W. Szott, C. Jedrezejek, and W.P. Kirk, Phys. Rev. B **40**, 1790 (1989), Supperlatt. Microstruct. **11**, 199 (1992).

[14] N. Cherradi, A. Audouard, G. Marchal, J.M. Broto, and A. Fert, Phys. Rev. B **39**, 7424 (1989); A. Audouard, A. Kazoun, J.M. Broto, G. Marchal, and A. Fert, Phys. Rev. B **42**, 2728 (1990).

[15] Y.B. Jin and J.B. Ketterson, Phys. Rev. B **33**, 8797 (1986).

[16] W. Szott, C. Jedrezejek, and W.P. Kirk, Phys. Rev. Lett. **63**, 1980 (1989).

[17] For isotropic three dimensional samples the WL contribution to the magnetoresistance is completely isotropic, and so therefore one would expect no difference between transverse and longitudinal geometries. However, our samples are anisotropic and also show a contribution from classical MR, and so this precaution is warranted.

[18] R.A. Hamm and J.M. Vandenberg, J. Appl. Phys. **56**, 293 (1984).

[19] H. Chen and S.M. Heald, Phys. Rev. B **42** 4913 (1990), J. Appl. Phys. **66**, 1793 (1989); S.M. Heald, H. Chen, and J.M. Tranquada, Phys. Rev. B **38**, 1016 (1988).

[20] D.V. Baxter, R. Richter, M.L. Trudeau, R.W. Cochrane, and J.O. Strom-Olsen, J. Phys. France **50**, 1673 (1989).

[21] R.W. Cochrane, B.J. Kastner, and W.B. Muir, J. Phys. E **15**, 425 (1982).

[22] C.M. Falco and I.K. Schuller in *Synthetically Modulated Structures*, edited by L.L. Chang, and B.C. Giessen (Academic, New York 1985), pp. 339-364.

[23] R. Richter, D.V. Baxter, and J.O. Strom-Olsen, Phys. Rev. B **38**, 10 421 (1988).

[24] J.B. Bieri, A. Fert, G. Creuzet, and A. Schuhl, J. Phys. F **16**, 2099 (1986).

[25] A.B. Pippard, *Magnetoresistance in Metals* (Cambridge University Press, New York, 1989).

[26] D. Belitz and S. Das Sarma, Phys. Rev. B **36**, 7701 (1987).

[27] A. Sahnoune, J.O. Strom-Olsen, and H.E. Fischer, Phys. Rev. B **46**, 10 035 (1992).

[28] H. Van Houten, C.W.J. Beenakker, B.J. Van Wees, and J.E. Mooij, Surf. Sci. **196**, 144 (1988); C.W.J. Beenakker and H. van Houten, Phys. Rev. B **38**, 3232 (1988).

[29] M. Gurvitch, Phys. Rev. B **34**, 540 (1986).

[30] E.E. Fullerton, I.K. Schuller, H. Vanderstraeten, and Y.

Bruynseraede, Phys. Rev. B **45**, 9292 (1992).
[31] S. Hikami, A.L. Larkin, and Y. Nagaoka, Prog. Theor. Phys. **63**, 707 (1980).
[32] A. Kawabata, J. Phys. Soc. Jpn. **49**, 628 (1980.)
[33] H. Fukuyama and K. Hoshino, J. Phys. Soc. Jpn. **50**, 2131 (1981).
[34] R.N. Bhatt, P. Wölfle, and T.V. Ramakrishnan, Phys. Rev. B **32**, 569 (1985).

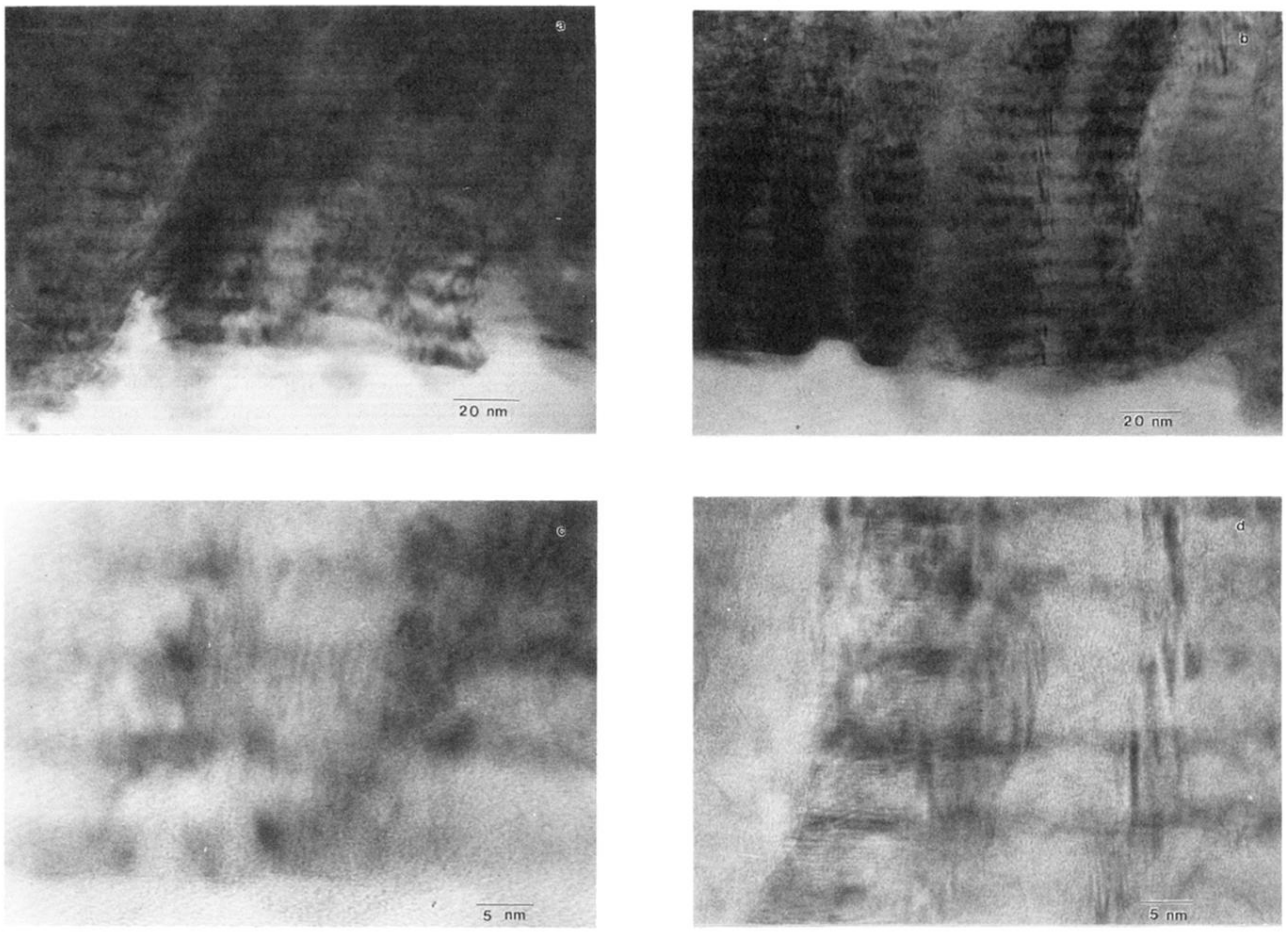

FIG. 11. Cross sectional TEM images of sample 1 [(a) and (c)] and sample 6 [(b) and (d)]. At lower magnification [(a) and (b)] we see that the structure in sample 6 is more stratified than is the case with sample 1, as expected for a sample showing greater anisotropy in its transport properties. In the higher magnification images greater coherence at the atomic level in sample 1 [figure (c)] is evident in the appearance of lattice fringes throughout the sample. In contrast to this, the lattice fringes observed in sample 6 [figure (d)] indicate some variation in the orientation of the crystals, revealing a lack of orientational coherence in this sample. This is consistent with the high angle x-ray diffraction results in 2(a).